

Nonlinear evolution equations in QCD [†]

Anna M. Stašto^(a,b)

^(a) *Nuclear Theory Group, Physics Department,
Brookhaven National Laboratory,
Upton, NY 11973, USA**

and

^(b) *H. Niewodniczański Institute of Nuclear Physics,
Polish Academy of Sciences,
ul. Radzikowskiego 152, 31-342 Kraków, Poland*

(November 8, 2018)

Abstract

The following lectures are an introduction to the phenomena of partonic saturation and nonlinear evolution equations in Quantum Chromodynamics. After a short introduction to the linear evolution, the problems of unitarity bound and parton saturation are discussed. The nonlinear Balitsky-Kovchegov evolution equation in the high energy limit is introduced, and the progress towards the understanding of the properties of its solution is reviewed. We discuss the concepts of the saturation scale, geometrical scaling and the lack of the infrared diffusion. Finally, we give a brief summary of current theoretical developments which extend beyond the Balitsky-Kovchegov equation.

1 Introduction

One of the most intriguing problems of Quantum Chromodynamics is the growth of cross sections for hadronic interactions at high energies. Let us consider the

[†]Presented at XLIV Cracow School of Theoretical Physics, June 2004, Zakopane, Poland.

*Permanent address.

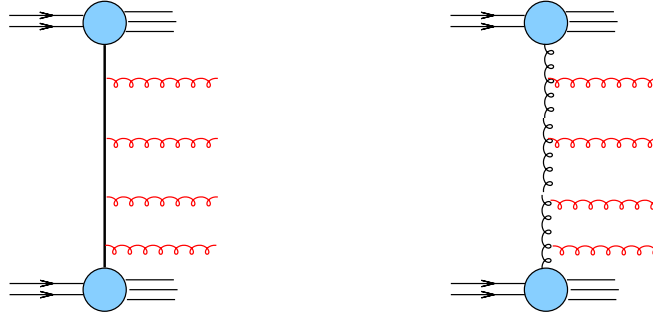


Figure 1: Scattering of two hadronic probes at high energy. Left: QED-type diagrams; right: diagrams with gluon self-interactions.

scattering of two particles at very high energy as shown in Fig.1. As the energy grows, so does the probability of emission of soft particles. In the case of QED one has to consider a diagram of the type shown on the left hand side graph in Fig. 1. In QCD one also encounters these diagrams, but there are also additional diagrams of the type shown on the right hand side of Fig. 1. Since gluons are the carriers of the color charge and couple to each other, the increase of energy causes a fast growth of the gluon density and, consequently, of the cross section. This increase leads to the formation of a dense, colored medium at very high energies.

In perturbative QCD the growth of the gluon density in the limit of high energy is governed by the BFKL Pomeron equation [1]. The solution to this equation gives a very strong, power-like growth of the gluon density, and of the resulting cross section

$$f(x) \sim x^{-\lambda},$$

where x is the Bjorken variable (a fraction of target's longitudinal momentum) and $\lambda = \frac{4 \ln 2 N_c}{\pi} \alpha_s$ is the intercept of the perturbative Pomeron in the leading logarithmic ($\text{LL}x, \ln 1/x \gg 1$) approximation. In the pioneering paper [2], Gribov, Levin and Ryskin pointed out that the gluon recombination is important at high energies. It reduces the growth of the parton density by producing an effect called the *perturbative partonic saturation*. In [2], a new nonlinear evolution equation in double leading logarithmic approximation (DLLA, $\ln 1/x \ln Q^2 \gg 1$) for the gluon density has been postulated. In addition to the gluon production it also takes into account the recombination effects

$$Q^2 \frac{\partial^2 xG(x, Q^2)}{\partial \ln 1/x \partial Q^2} = \frac{\alpha_s N_c}{\pi} xG(x, Q^2) - \frac{4\alpha_s^2 N_c}{3C_F R^2} \frac{1}{Q^2} [xG(x, Q^2)]^2. \quad (1)$$

Note the negative sign in front of the nonlinear term responsible for the gluon recombination. The strong growth generated by the linear term is damped for large gluon densities $xG(x, Q^2)$ (of the order $1/\alpha_s$).

Partonic saturation plays also an important role in the context of the unitarity bound. It is well known that the hadronic cross sections obey the Froissart bound [3] which stems from the general assumptions of the analyticity and unitarity of the scattering amplitude. The Froissart bound implies that the total cross section does not grow faster than the logarithm squared of the energy

$$\sigma_{tot} = \frac{\pi}{m_\pi^2} (\ln s)^2, \quad (2)$$

where m_π is the scale of the range of the strong force. It is generally believed, that the parton saturation mechanism leads to the unitarization of the cross section at high energies. Unfortunately, the problem is quite complex since the parton saturation is purely perturbative mechanism while the Froissart bound has been derived from general principles and it refers to the QCD as to a complete theory of strong interactions (including the nonperturbative effects). The GLR postulate resulted in increased efforts to develop a theory able to describe the saturation at high energies. One effective theory for high density partonic systems at small x is the Color Glass Condensate [4] with the resulting JIMWLK evolution equations [5, 6]. Another approach has been developed by Balitsky [7] who constructed an infinite hierarchy of coupled equations for correlators of Wilson lines. In the mean field approximation the first equation of this theory decouples, and is equivalent to the Kovchegov equation [8] (derived independently in the dipole approach [9]). The Kovchegov equation is a nonlinear equation for the dipole scattering amplitude valid in the leading $\log 1/x$ approximation. The Balitsky-Kovchegov (BK) equation is perhaps the best known equation that includes the saturation effects and has a virtue that it can be relatively simply solved, at least numerically.

The goal of the following lecture is to introduce the reader into the phenomenon of the partonic saturation and nonlinear evolution using BK equation as an example. We shall start with a brief review of the linear evolution in QCD. Then we shall recall the Froissart bound and the necessary conditions for its derivation. Then the properties of the solution of the BK equation will be investigated with particular emphasis on the the infrared diffusion, saturation scale and the geometrical scaling. We will continue with an analysis of this equation in general case in 4 dimensions, which takes into account the dipole spatial distribution in the impact parameter space. We will conclude with a short outlook and the discussion of recent theoretical developments in the field.

2 DIS kinematics and variables

Let us concentrate on the deep inelastic scattering process of lepton off the hadron or nucleus. For completeness, let us first recall the basic kinematic features of DIS, as represented in Fig. 2. The total energy squared of the electron-nucleon system is $s_{(eN)} = (p+k)^2$, whereas that of the photon-nucleon system is $s_{\gamma^*N} = (p+q)^2$. The photon virtuality is denoted by $q^2 = (k-k')^2 = -Q^2 < 0$ and the Bjorken variable $x = \frac{Q^2}{2p \cdot q} = \frac{Q^2}{Q^2 + s_{(\gamma^*N)}}$.

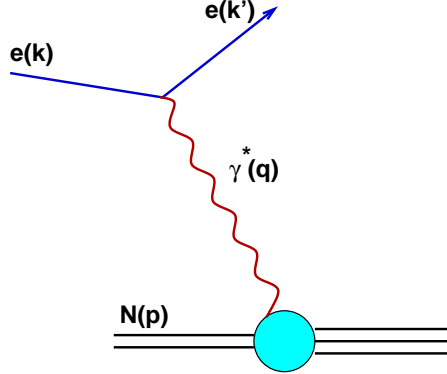


Figure 2: Deep inelastic scattering process of electron on the hadronic target.

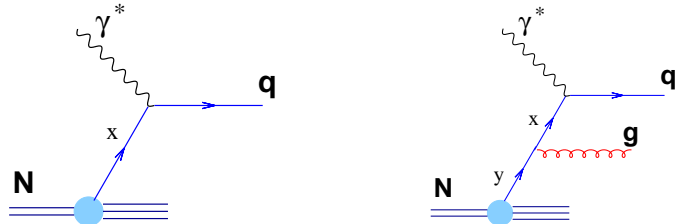


Figure 3: Left: photon with virtuality Q^2 probes quark with a longitudinal momentum fraction x . Right: the virtuality (resolution) is increased so the density of quarks also grows.

The high energy regime, is defined as

$$\begin{aligned}
 s_{(\gamma^* N)} &\longrightarrow \infty, \\
 x &= \frac{Q^2}{Q^2 + s_{(\gamma^* N)}} \simeq \frac{Q^2}{s_{(\gamma^* N)}} \longrightarrow 0, \\
 Y &= \ln 1/x \longrightarrow \infty.
 \end{aligned} \tag{3}$$

3 The linear evolution equations of QCD

Let us consider a scattering of photon with virtuality Q^2 off a hadron at center of mass energy \sqrt{s} . The photon virtuality defines a resolution scale $\lambda \sim \frac{1}{\sqrt{Q^2}}$ with which one probes the partonic structure of a hadron, see the left hand side graph in Fig. 3. At a given resolution $t = \ln Q^2/Q_0^2$, the photon probes the density of partons $q(x, t)$ with a fraction of the hadron momentum $x = Q^2/s$. By increasing Q^2 one also increases the resolution, and the density of quarks is larger: $q(x, t) + \delta q(x, t)$, see right-hand graph in Fig. 3. The underlying process

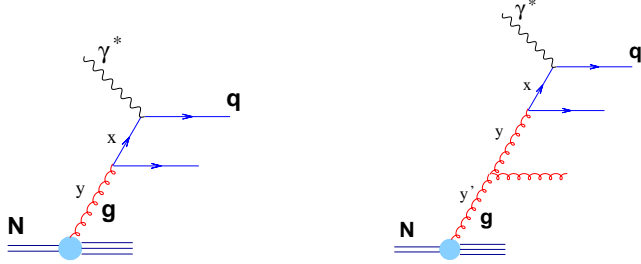


Figure 4: Additional set of diagrams present in the DGLAP evolution.

can be described by the following linear evolution equation for density

$$\frac{\partial q(x, t)}{\partial t} = \frac{\alpha_s(t)}{2\pi} \int_x^1 \frac{dy}{y} P_{qq}(x/y) q(y, t). \quad (4)$$

The splitting function $P_{qq}(z = x/y)$ describes the probability of finding a quark inside the parent quark, with a fraction $z = x/y$ of the parent quark momentum. This is one of the set of the well known DGLAP evolution equations [10]. For the DGLAP equations to be complete, apart from the quark density $q(x, t)$, one has to include the gluon density $g(x, t)$ coupled to q . The evolution of the gluon density is shown in Fig. 4. The full set of singlet DGLAP equations reads as

$$\frac{\partial}{\partial t} \begin{bmatrix} \Sigma(x, t) \\ g(x, t) \end{bmatrix} = \frac{\alpha_s(t)}{2\pi} \begin{bmatrix} P_{qq} & 2N_f P_{qg} \\ P_{gg} & P_{gg} \end{bmatrix} \stackrel{x}{\otimes} \begin{bmatrix} \Sigma(x, t) \\ g(x, t) \end{bmatrix},$$

where $\Sigma(x, t) = \sum_i [q_i(x, t) + \bar{q}_i(x, t)]$ is the singlet quark density.

An alternative approach to DGLAP [1] is to consider a fixed virtuality of the probe and to increase the energy s (or alternatively rapidity Y), see Fig. 5. This procedure leads to the BFKL equation

$$\frac{\partial G(x, t)}{\partial \ln 1/x} = \frac{\alpha_s N_c}{\pi} \int dt' \mathcal{K}(t, t') G(x, t'), \quad (5)$$

which is an evolution equation in Bjorken x . The quantity $\mathcal{K}(t, t')$ (Lipatov kernel) describes the probability of branching of the gluon with virtuality t' into another gluon with virtuality t . The function $G(x, t)$ is called the unintegrated gluon density and is related to $g(x, t)$ by

$$g(x, t) = \int^t dt' G(x, t').$$

Both \mathcal{K} and P_{ij} have perturbative expansions in α_s and share a finite number of common terms in the expansion. The solution to the BFKL equation has the form, see for example [11]

$$G(x) \sim x^{-\lambda_P}, \quad \lambda_P = 4 \ln 2N_c \alpha_s / \pi. \quad (6)$$

This solution strongly grows with $1/x$ (and, correspondingly with energy $s = Q^2/x$) which contradicts the Froissart bound [3].

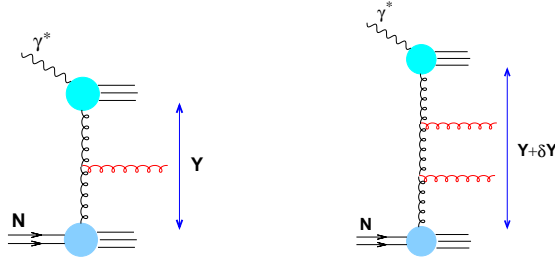


Figure 5: Evolution in the BFKL framework: virtualities of probes are fixed and energy is increased.

4 Froissart bound

Let us recall the basic assumptions used in the derivation of the Froissart bound [3]. This bound applies for the total cross section for scattering of two hadrons, and reads as follows

$$\sigma_{\text{TOT}} \leq \frac{\pi}{m_\pi^2} (\ln s)^2. \quad (7)$$

Its derivation is based on two assumptions: the unitarity of partial amplitudes and the finite length of the strong interaction. The first condition demands that the S matrix has to be unitary

$$S^\dagger S = S S^\dagger = 1. \quad (8)$$

A set of particle states $|m\rangle$ has to satisfy completeness relation

$$\sum_m |m\rangle \langle m| = 1. \quad (9)$$

Then the probability that the initial state $|i\rangle$ evolves into the final state $|f\rangle$ is

$$P_{fi} = |\langle f | S | i \rangle|^2. \quad (10)$$

Since a probability that a given final state comes from any initial state is 1 therefore the sum of these probabilities over all the initial states equals 1

$$\sum_f P_{fi} = \langle i | S^\dagger S | i \rangle = 1, \quad (11)$$

which is interpreted as a unitarity condition for the S -matrix (8).

The second assumption is on the finite range R of strong force determined by the mass scale m_π

$$R \sim \frac{1}{m_\pi}, \quad (12)$$

which determines the cutoff. The scale m_π is entirely nonperturbative. The Froissart bound can be derived [3] by using these two assumptions and the

Mandelstam representation. One has to stress that the Froissart bound is applicable to the complete QCD theory that includes both perturbative and non-perturbative parts.

It is worthwhile to mention that while one believes that Froissart bound is valid, it is not immediately visible from the data. The data show that the structure function for deep inelastic scattering at high photon virtualities strongly rises with decreasing x , consistent with a power behaviour $x^{-\lambda}$ with $\lambda \simeq 0.35$. Further, the data show no sign of a logarithmic dependence is seen, see Fig. 6.

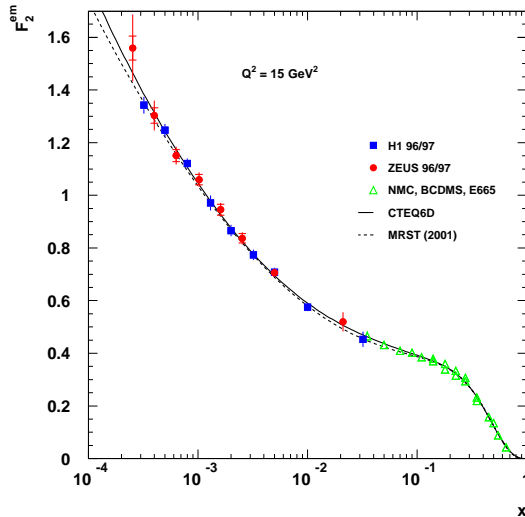


Figure 6: F_2 structure function data from HERA collider and fixed target experiments.

Pinning down the saturation effects in experimental data is a nontrivial task. A specific problem with the structure function data is that it involves completely inclusive measurements. In particular, structure function F_2 is averaged over the impact parameter of the $\gamma^* - p$ collision. It is also known that saturation effects crucially depend on this variable. Therefore the search for the saturation should involve more exclusive processes, e.g. diffraction. For more information on the saturation phenomenology consult [12, 13] and references therein.

5 Parton saturation and nonlinear evolution

Given that the Froissart bound should be satisfied, a natural question arises: how to modify the perturbative evolution in order to tame the growth of the cross section? One would like to identify the Feynman diagrams which are

responsible for gluon recombination and to derive the appropriate evolution equations that include these diagrams. As already stated in the introduction, the standard evolution equations lead to a strong rise of the parton density in high energy limits. One can expect that partons overlap when their density becomes large. The schematic picture of the saturation phenomenon is shown in Fig. 7.

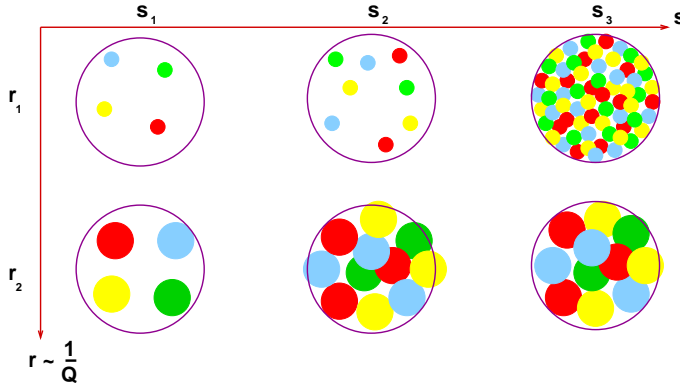


Figure 7: Schematic view of parton saturation. Horizontal axis is energy squared s , the vertical axis is r , the parton size.

The horizontal axis represents the energy whereas and the vertical one the parton size defined by the inverse of the photon virtuality $r \sim 1/Q$ in the deep inelastic scattering process. The onset of saturation depends on energy and on the parton size. The larger the size of the partons, the earlier they fill up the available area and start to reinteract. A further increase of the energy will not increase the probed parton density. Therefore, apart from production diagrams, one has to include additional diagrams which take into account gluon recombination. This leads to the modification of the evolution equation by a term which is nonlinear in density. The first equation of this type was the GLR equation [2]

$$Q^2 \frac{\partial^2 xG(x, Q^2)}{\partial \ln 1/x \partial Q^2} = \frac{\alpha_s N_c}{\pi} xG(x, Q^2) - \frac{4\alpha_s^2 N_c}{3C_F R^2} \frac{1}{Q^2} [xG(x, Q^2)]^2. \quad (13)$$

The first term in (13) is the usual DGLAP term in the double logarithmic approximation, $\ln 1/x \ln Q^2/\Lambda^2 \gg 1$, whereas the second, nonlinear, term is responsible for gluon recombination. The nonlinear term is inversely proportional to the hadron area $\sim R^2$ and the scale $\sim Q^2$ at which the gluon density is probed. The smaller the hadron area, the earlier the partons fill it up and saturate. The scale Q^2 defines the parton size $r \sim 1/Q$. For small values of r the saturation is delayed to larger energies.

The GLR equation sums a subset of diagrams within the double leading logarithmic approximation. They are called *fan diagrams*, and are illustrated on the right hand graph in Fig. 8.

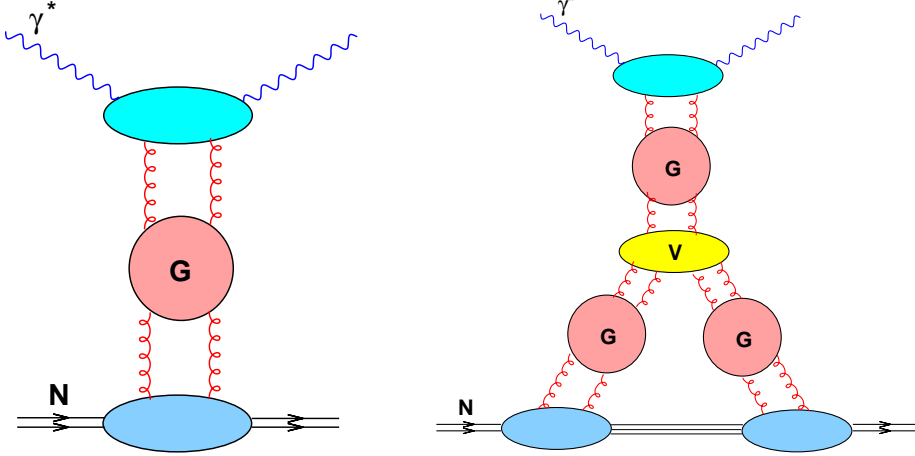


Figure 8: Left: linear evolution. Right: fan diagrams summed by the nonlinear GLR equation (13).

The nonlinear Balitsky-Kovchegov (BK) equation is valid in the leading logarithmic $\ln 1/x$ approximation. It has been derived independently by Kovchegov [8] within the dipole formulation of high energy scattering and by Balitsky [7] from the operator product expansion for high energy scattering. More precisely, Balitsky's equations form an infinite hierarchy of coupled equations for correlators of Wilson lines, and only in the mean field approximation the first equation decouples and is equivalent to the equation derived by Kovchegov. An independent approach is that of Color Glass Condensate [4] in which the evolution is governed by the JIMWLK functional equation [5] equivalent to Balitsky hierarchy. In this lecture we will study the solution of the Balitsky-Kovchegov equation which is currently the simplest tool to describe the parton saturation phenomenon.

6 Multiple scattering in dipole picture

In this section we will follow the derivation of the BFKL [9] and BK [8] equations in the dipole picture. Consider a heavy quark-antiquark pair, *onium*, shown in Fig. 9, who's wave function in the momentum space is denoted by

$$\psi_{\alpha\beta}^{(0)}(k_1, z_1),$$

where k_1 is the transverse momentum of the quark and $z_1 = \frac{k_{1+}}{p_+}$ is the fraction of light cone momentum carried by the quark.

The dipole picture is formulated by going to the transverse coordinate space

$$\psi_{\alpha\beta}^{(0)}(\mathbf{x}_0, \mathbf{x}_1, z_1) = \int \frac{d^2 \mathbf{k}_1}{(2\pi)^2} e^{i\mathbf{x}_0 \cdot \mathbf{k}_1} \psi_{\alpha\beta}^{(0)}(\mathbf{k}_1, z_1),$$

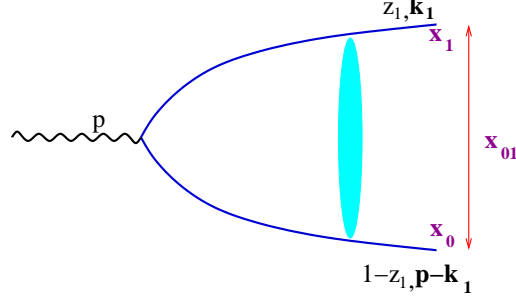


Figure 9: Heavy quark-antiquark dipole *onium*.

$$\Phi^{(0)}(\mathbf{x}_0, \mathbf{x}_1, z_1) = \sum_{\alpha, \beta} |\psi_{\alpha\beta}^{(0)}(\mathbf{x}_0, \mathbf{x}_1, z_1)|^2 ,$$

where $\mathbf{x}_0, \mathbf{x}_1$ denote the positions of the quark and antiquark respectively, which form the end points of the *dipole*.

Then, as shown in Fig. 10, one adds one soft gluon with its longitudinal momentum much smaller than that of the original quark (anti-quark) $z_2/z_1 \ll 1$

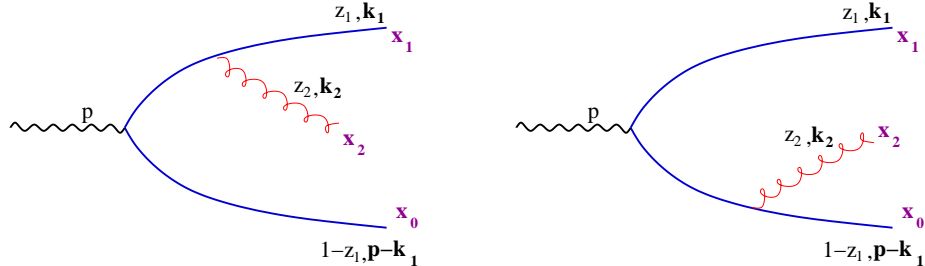


Figure 10: Onium with an additional single soft gluon.

The relation between the one-gluon wave function $\Phi^{(1)}$ and onium wave function without any soft gluons $\Phi^{(0)}$ is

$$\Phi^{(1)}(\mathbf{x}_0, \mathbf{x}_1, z_1) = \frac{\alpha_s C_F}{\pi^2} \int_{z_0}^{z_1} \frac{dz_2}{z_2} \int d^2 \mathbf{x}_2 \frac{\mathbf{x}_{01}^2}{\mathbf{x}_{20}^2 \mathbf{x}_{12}^2} \Phi^{(0)}(\mathbf{x}_0, \mathbf{x}_1, z_1) .$$

In the limit of large number of colors, the gluon can be represented by a quark-antiquark pair, as in Fig. 11. The emission of one additional gluon is equivalent to the splitting of the original dipole $(0, 1)$ into two dipoles $(0, 2)$ and $(2, 1)$ with probability of branching given by the measure

$$d^2 \mathbf{x}_2 \frac{\mathbf{x}_{01}^2}{\mathbf{x}_{20}^2 \mathbf{x}_{12}^2} .$$

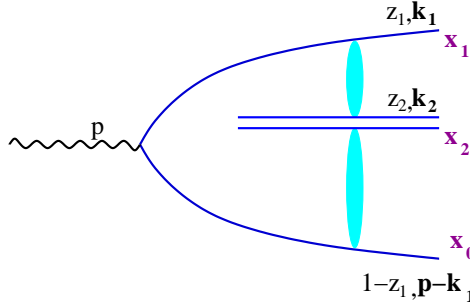


Figure 11: Onium wave function which consists of two dipoles.

The process of emissions of subsequent soft dipoles can be repeated in the analogous way to obtain the wave function with an arbitrary number of gluons $\Phi^{(n)}$, see Fig. 12. To describe such a process, Mueller [9] introduced a dipole generating functional

$$Z(\mathbf{b}_{01}, \mathbf{x}_{01}, z_1, u) ,$$

which satisfies the normalization condition

$$Z(\mathbf{b}_{01}, \mathbf{x}_{01}, z_1, u = 1) = 1 .$$

The wave functions for arbitrary number of gluons can be obtained by performing functional differentiation of Z ,

$$\Phi^{(n)}(\mathbf{x}_0, \mathbf{x}_1, \mathbf{x}_2, \dots, \mathbf{x}_{n+1}) = \Phi^{(0)} \frac{\delta}{\delta u(\mathbf{x}_2)} \frac{\delta}{\delta u(\mathbf{x}_3)} \cdots \frac{\delta}{\delta u(\mathbf{x}_{n+1})} Z(\mathbf{x}_0, \mathbf{x}_1, z_1, u)|_{u=0} .$$

Here $\Phi^{(n)}$ gives probability of finding n daughter dipoles that originate from parent quark-antiquark dipole $(0, 1)$. The daughter dipoles are produced in positions x_k with $k = 2, \dots, n$. In the following, we will use another notation with

$$\mathbf{x}_{01} \equiv \mathbf{x}_0 - \mathbf{x}_1 ,$$

representing the transverse size of the dipole and

$$\mathbf{b}_{01} \equiv \frac{\mathbf{x}_0 + \mathbf{x}_1}{2} ,$$

the impact parameter (position) of this dipole.

By investigating the relation between wave functions with n and $n+1$ dipoles Mueller derived [9] the following differential equation for the generating functional

$$\begin{aligned} \frac{dZ(\mathbf{b}_{01}, \mathbf{x}_{01}, y, u)}{dy} = & \\ \int \frac{d^2 \mathbf{x}_2 \mathbf{x}_{01}^2}{\mathbf{x}_{20}^2 \mathbf{x}_{12}^2} & \left[Z\left(\mathbf{b}_{01} + \frac{\mathbf{x}_{12}}{2}, \mathbf{x}_{20}, y, u\right) Z\left(\mathbf{b}_{01} - \frac{\mathbf{x}_{20}}{2}, \mathbf{x}_{12}, y, u\right) - Z(\mathbf{b}_{01}, \mathbf{x}_{01}, y, u) \right] , \end{aligned} \quad (14)$$

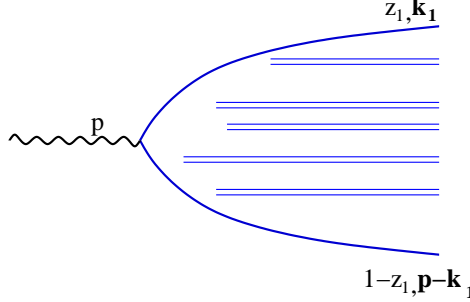


Figure 12: Onium wave function with arbitrary number of dipoles.

where the evolution variable is the rapidity $y = \ln 1/z_+$. Using equation (14), one can obtain the evolution equation for the scattering amplitude of dipole on the target. First, one constructs the dipole number density

$$n_1(x_{01}, \mathbf{x}, \mathbf{b} - \mathbf{b}_0, Y) = \frac{\delta}{\delta u(\mathbf{b}, \mathbf{x})} Z(\mathbf{b}_{01}, \mathbf{x}_{01}, Y, u)|_{u=1},$$

and in general, the density for k dipoles

$$n_k = \prod_{i=1}^k \frac{\delta}{\delta u(\mathbf{b}_i, \mathbf{x}_i)} Z|_{u=1}. \quad (15)$$

The amplitude for scattering of single dipole on a target, see left graph in Fig. 13, can be then obtained by convoluting the dipole number density with the propagator of that dipole in the nucleus

$$N_1(\mathbf{x}_{01}, \mathbf{b}_{01}, Y) = \int d[\mathcal{P}_1] n_1 \gamma_1, \quad (16)$$

where $d[\mathcal{P}]_1 = \frac{d^2 \mathbf{x}_1}{2\pi x_1^2} d^2 \mathbf{b}_1$ is the phase space measure, and $\gamma \equiv \gamma(\mathbf{x}, \mathbf{b})$ is the propagator of a single dipole in the nucleus. By differentiating the equation for the generating functional and using the relation (16) one can obtain the linear evolution equation for the dipole-target amplitude

$$\frac{dN_1(\mathbf{b}_{01}, \mathbf{x}_{01}, Y)}{dY} = \bar{\alpha}_s \int \frac{d^2 \mathbf{x}_2 x_{01}^2}{\mathbf{x}_{20}^2 \mathbf{x}_{12}^2} \left[N_1(\mathbf{b}_{01} + \frac{\mathbf{x}_{12}}{2}, \mathbf{x}_{20}, Y) + N_1(\mathbf{b}_{01} - \frac{\mathbf{x}_{20}}{2}, \mathbf{x}_{12}, Y) - N_1(\mathbf{b}_{01}, \mathbf{x}_{01}, Y) \right]. \quad (17)$$

It has to be stressed that only the contribution from the *single scattering* of one dipole on the target has been included in the derivation. The equation (17) is a dipole version of the BFKL equation in the transverse coordinate space as derived in [9]. One can also generalize this equation by taking into account a

multiple scattering of many dipoles on the target, see right graph in Fig. 13. To this aim one takes the number density of k dipoles, Eq. (15), and then convolutes it with k propagators for respective dipoles. The following expression for the amplitude is then

$$N(\mathbf{x}_{01}, \mathbf{b}_{01}, Y) = \sum_{k=1}^{\infty} \int d[\mathcal{P}_k] n_k \gamma_1 \dots \gamma_k , \quad (18)$$

where the measure is defined as

$$[\mathcal{P}]_k = \Pi_{i=1}^{i=k} \frac{d^2 \mathbf{x}_i}{2\pi x_i^2} d^2 \mathbf{b}_i .$$

By differentiation of the equation for the generating functional Z one can obtain the evolution equation for the amplitude which takes into account also multiple scatterings [8]

$$\frac{dN(\mathbf{b}_{01}, \mathbf{x}_{01}, Y)}{dY} = \bar{\alpha}_s \int \frac{d^2 \mathbf{x}_2 \mathbf{x}_{01}^2}{\mathbf{x}_{20}^2 \mathbf{x}_{12}^2} \left[N(\mathbf{b}_{01} + \frac{\mathbf{x}_{12}}{2}, \mathbf{x}_{20}, Y) + N(\mathbf{b}_{01} - \frac{\mathbf{x}_{20}}{2}, \mathbf{x}_{12}, Y) - N(\mathbf{b}_{01}, \mathbf{x}_{01}, Y) - N(\mathbf{b}_{01} + \frac{\mathbf{x}_{12}}{2}, \mathbf{x}_{20}, Y) N(\mathbf{b}_{01} - \frac{\mathbf{x}_{20}}{2}, \mathbf{x}_{12}, Y) \right] . \quad (19)$$

The characteristic feature of this equation is its nonlinearity. Thus, in the dipole approach, the multiple scattering of many dipoles in the onium leads to nonlinear evolution equation for the amplitude. This has to be contrasted with the single scattering of one dipole which leads to the linear BFKL-type equation. One has to stress that this multiple scattering is a completely incoherent process:

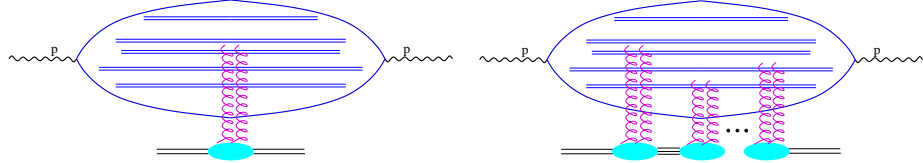


Figure 13: Left: single dipole scattering which leads to linear BFKL evolution equation (17). Right: multiple dipole scattering which results in nonlinear Balitsky-Kovchegov evolution equation (19).

dipoles scatter independently of each other and there are no correlations. This is quite an important simplification which results in a relatively simple and closed evolution equation. These correlations are now a subject of intensive research.

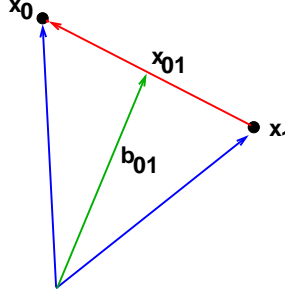


Figure 14: Schematic representation of the dipole position in impact parameter space. $(\mathbf{x}_0, \mathbf{x}_1)$ denote end points of the dipole.

7 Balitsky-Kovchegov equation at high energies

In the remaining sections of the paper will be devoted to the discussion of the solutions to the BK equation

$$\frac{dN(\mathbf{b}_{01}, \mathbf{x}_{01}, Y)}{dY} = \bar{\alpha}_s \int \frac{d^2 \mathbf{x}_2 \mathbf{x}_{01}^2}{\mathbf{x}_{20}^2 \mathbf{x}_{12}^2} \left[N(\mathbf{b}_{01} + \frac{\mathbf{x}_{12}}{2}, \mathbf{x}_{20}, Y) + N(\mathbf{b}_{01} - \frac{\mathbf{x}_{20}}{2}, \mathbf{x}_{12}, Y) - N(\mathbf{b}_{01}, \mathbf{x}_{01}, Y) - N(\mathbf{b}_{01} + \frac{\mathbf{x}_{12}}{2}, \mathbf{x}_{20}, Y) N(\mathbf{b}_{01} - \frac{\mathbf{x}_{20}}{2}, \mathbf{x}_{12}, Y) \right]. \quad (20)$$

Let us highlight the salient features of this equation:

- i) BK equation is an evolution equation in rapidity $Y = \ln 1/x$.
- ii) It requires the initial conditions $N^{(0)}(\mathbf{b}_{01}, \mathbf{x}_{01}, Y = 0)$ which depend on the target of the specific process to be specified.
- iii) The BK equation is valid in the leading logarithmic approximation in which the powers in $(\alpha_s \ln 1/x)^n$ are counted.
- iv) In this approximation the strong coupling α_s is fixed.
- v) In (20) \mathbf{b}_{01} represents the impact parameter whereas \mathbf{x}_{01} is the size of the dipole, see Fig. 14. The problem involves $(4 + 1)$ variables: four degrees of freedom per dipole and one evolution variable.

7.1 Toy model in $(0 + 1)$ dimensions

Searching for the solutions to Eq. (20) one has first to notice that this equation has two fixed points

$$\frac{dN(\mathbf{b}_{01}, \mathbf{x}_{01}, Y)}{dY} = 0,$$

which are at

$$N = 0 \quad \text{and} \quad N = 1.$$

It is quite instructive to first investigate the toy model in $(0 + 1)$ dimensions, when amplitude depends only on the rapidity $N \equiv N(Y)$ and the kernel is

simply a constant. Then the equation reduces to

$$\frac{dN}{dY} = \omega(N - N^2), \quad \omega > 0.$$

The above equation was first discussed by Verhulst in 1838 as a model for self-limiting population growth in biology. The solution to this equation, called logistic curve, can be easily found

$$N(Y) = \frac{e^{\omega Y}}{e^{\omega Y} + C^{-1}}, \quad N^{(0)}(Y = 0) = C,$$

and is illustrated in Fig. 15. Its crucial property is that it saturates for very large values of Y

$$\forall_{C \neq 0} N(Y) \xrightarrow{Y \rightarrow \infty} 1,$$

in contrast to the solution of the linear equation which grows exponentially.

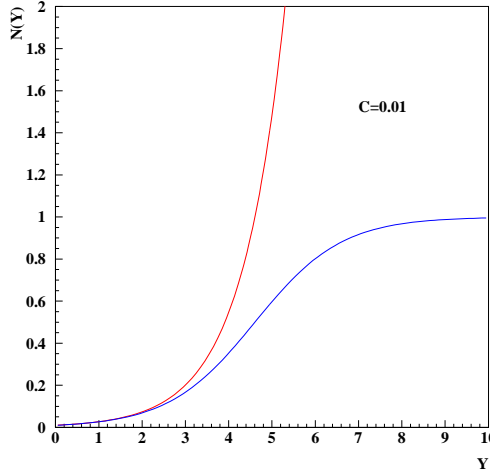


Figure 15: Illustration of the solution to the Verhulst equation (saturated line) and the linear equation (exponentially increasing).

The toy model teaches us that the fixed point at $N = 0$ is unstable with respect to the linear part of the evolution. In contradistinction, the value of $N = 1$ turns out to be a fixed point. After sufficiently long evolution in Y the solution will reach this fixed point, independently of initial conditions (provided that $N^{(0)}(Y = 0) \neq 0$).

8 Solution in $(1 + 1)$ dimensions

Having briefly looked at the toy model let us proceed to the full equation which depends on $(4 + 1)$ variables which makes it very difficult to solve even numeri-

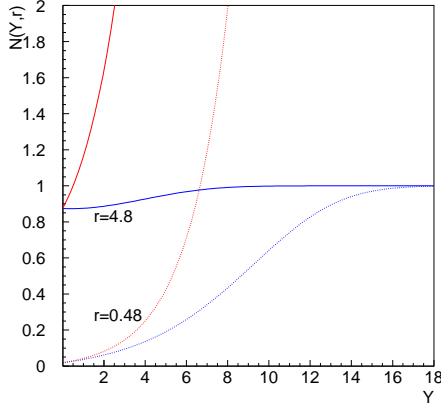


Figure 16: Rapidity dependence of the solution to $(1+1)$ dimensional Balitsky-Kovchegov equation (saturated lines) for two, fixed values of the dipole size r as compared to the solution of the linear BFKL equation (exponentially increasing).

callly. The biggest complication is that the variables \mathbf{b}_{01} and \mathbf{x}_{01} are entangled in the arguments of the functions N , see Eq.(20). However, the kernel depends only on the sizes $\mathbf{x}_{01}, \mathbf{x}_{20}, \mathbf{x}_{12}$. By assuming that the solution N is translationally invariant

$$N(\mathbf{b}_{01}, \mathbf{x}_{01}, Y) \rightarrow N(|\mathbf{x}_{01}|, Y) ,$$

the problem is reducible to $(1+1)$ dimensions with no dependence on the impact parameter \mathbf{b}_{01} . Physically, this corresponds to scattering of a dipole on an infinite and uniform nucleus. In this approximation, the BK equation in $(1+1)$ dimensions has been extensively studied numerically, [14, 15, 16, 17] and analytically [18, 19, 20].

In Fig. 16 we illustrate the rapidity dependence of $N(Y, r = |\mathbf{x}_{01}|)$ for two fixed values of r , and compare it to the solution of the linear equation. We notice that the solution to the BK equation has the same qualitative features as the toy model. For any given r the solution of the nonlinear equation tends to unity, whereas the linear solution increases exponentially.

Also when the dipole size is larger, the system also saturates earlier, for smaller values of Y . To understand this feature better let us look at the solution as a function of the dipole size r for given, fixed values of Y . We notice that for smaller dipoles the amplitude $N = 1$ as the rapidity increases. In the following, see Fig. 17, we will also study the dependence of N on different initial conditions.

In Fig. 17 several initial conditions have been shown. They require different normalisations and exhibit different type of behaviour for large values of r ($N(r) \rightarrow 1$ or $N(r) \rightarrow 0$ as $r \rightarrow \infty$). In all cases the common feature of the solution is that $N = 0$ is an unstable fixed point and $N = 1$ is the stable one.

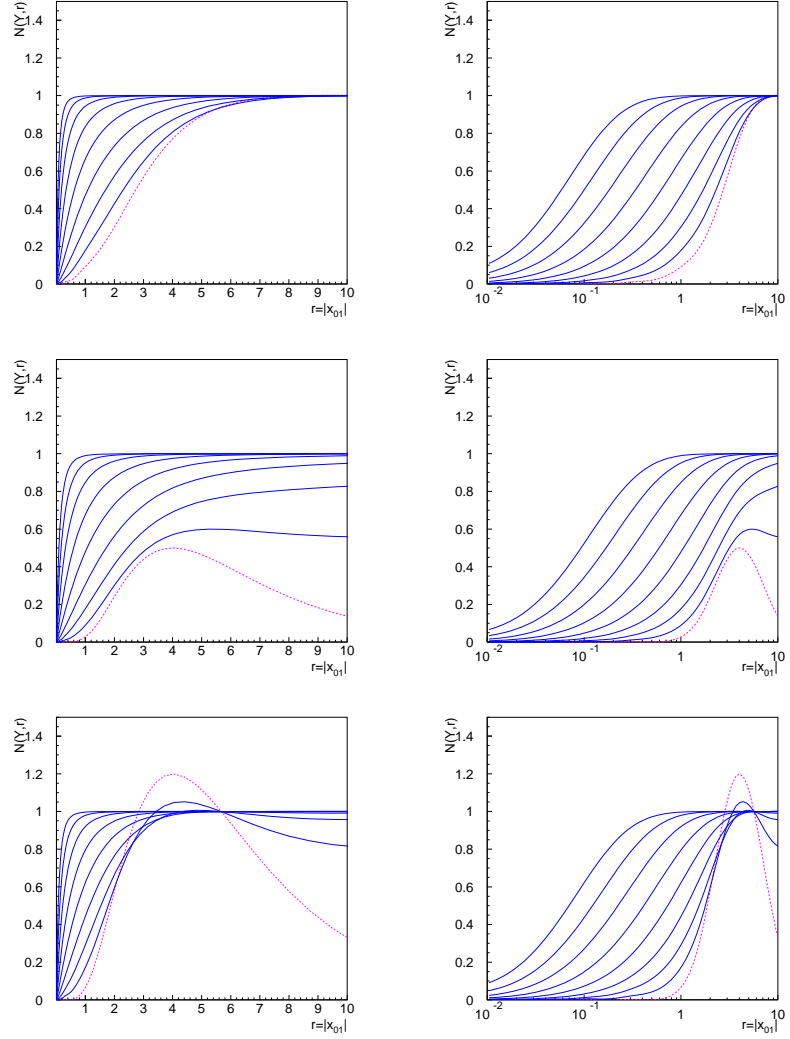


Figure 17: Dipole size dependence of the solution to the $(1+1)$ dimensional Balitsky-Kovchegov equation for different values of rapidity. From top to bottom: different initial conditions; left: linear scale; right: logarithmic scale. Dashed line denotes the initial distribution at $Y = 0$. Solid lines from right to left are for increasing values of rapidity.

8.1 Saturation scale

The solutions shown in Fig. 17 exhibit three different behaviours : in one region where the amplitude is small the nonlinear corrections are negligible, the transition region and the asymptotic region where the amplitude $N \sim 1$. The boundary of the transition region is characterized by a saturation scale $Q_s(Y)$

$$\begin{aligned} r < \frac{1}{Q_s(Y)} &\rightarrow N \ll 1 \text{ to the left} , \\ r > \frac{1}{Q_s(Y)} &\rightarrow N \sim 1 \text{ to the right} . \end{aligned}$$

The saturation scale can be extracted from the solution to the BK equation. The leading rapidity dependence is exponential

$$Q_s(Y) = Q_0 \exp(\bar{\alpha}_s \lambda Y) Y^{-\beta}, \quad \lambda \simeq 2.4 ,$$

with some subleading corrections [21, 19].

The qualitative properties of the BK equation are roughly similar to the properties of the dipole cross section of the Golec-Biernat and Wusthoff saturation model [13] in which the following form of the dipole cross section has been postulated

$$\sigma(Y, r) \equiv \int d^2\mathbf{b} N(\mathbf{b}, r, Y) = \sigma_0 \left[1 - \exp \left(-\frac{r^2 Q_s^2(Y)}{4} \right) \right] . \quad (21)$$

In (21) the saturation scale: $Q_s^2(Y) = e^{0.28(Y - Y_0)}$ is rapidity dependent. The normalisation σ_0 has been adjusted to obtain the best description of the experimentally measured proton structure function F_2 . In the regime where dipoles are smaller than the reciprocal of the characteristic saturation scale $r < 1/Q_s(Y)$, the cross section is small and proportional to

$$\sigma(r, Y)/\sigma_0 \simeq r^2 Q_s^2(Y)/4 ,$$

in accordance with the requirement of color transparency. When we consider large dipoles, $r > 1/Q_s(Y)$, the cross section saturates to σ_0

$$\sigma(r, Y)/\sigma_0 \simeq 1 ,$$

and becomes independent of both r and Y .

8.2 Geometrical scaling and travelling waves

While investigating the solution as a function of the dipole size r one observes that the solution reaches the universal shape independently of the particulars of the initial condition. For different values of Y the solutions have similar shapes but are shifted towards smaller values of the dipole size. This property is known as *geometrical scaling* and it was first searched for and found in the

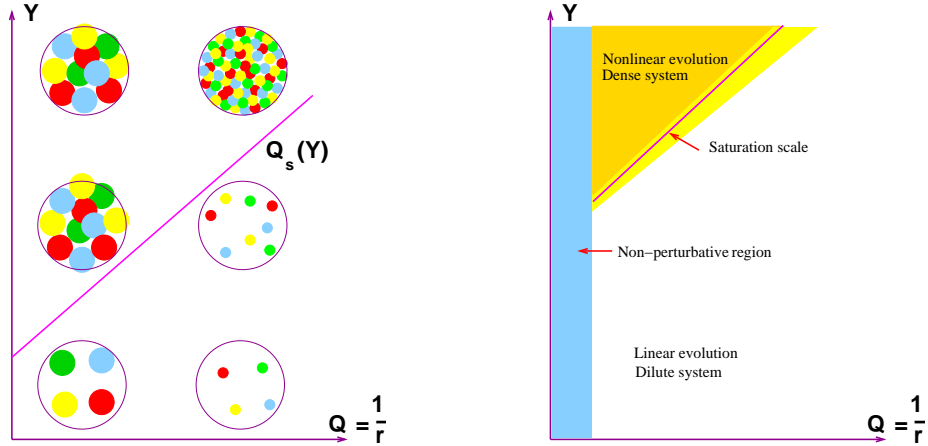


Figure 18: Schematic representation of dilute and saturated regions regions in the kinematic space (Q, Y) .

data at HERA electron-proton collider [22, 23]. Mathematically, geometrical scaling means that the solution to the BK equation depends only on a single combined variable

$$rQ_s(Y) ,$$

instead of r and Y separately, i.e.

$$N(r, Y) \equiv N(rQ_s(Y)) .$$

In terms of logarithms of variables, using the rapidity dependence of the saturation scale $Q_s(Y) \simeq Q_0 \exp(\bar{\alpha}_s \lambda_s Y)$ one finds that

$$\ln r + \ln Q_s(Y) = \ln r + \bar{\alpha}_s \lambda_s Y .$$

If we interpret $\ln r$ as a spatial coordinate and Y as the time variable, then the property of geometrical scaling implies that the solution is a wave front that propagates with a constant velocity $\bar{\alpha}_s \lambda_s$, see [19]. It has been also described as a soliton wave [14]. The scaling property is also present in the Golec-Biernat and Wusthoff saturation model (21).

The transition between the dilute and saturated regimes can be illustrated as in Fig. 18. The dense and dilute regions are divided by the critical line identified as the saturation scale. The higher the rapidity the denser the system becomes and finally partons begin to reinteract. The saturation occurs earlier also, for the larger size of the partons.

9 Diffusion properties of the BK equation

Insofar we have looked at the solutions in the coordinate space in accordance with the original formulation of the BK theory. By Fourier transform to the

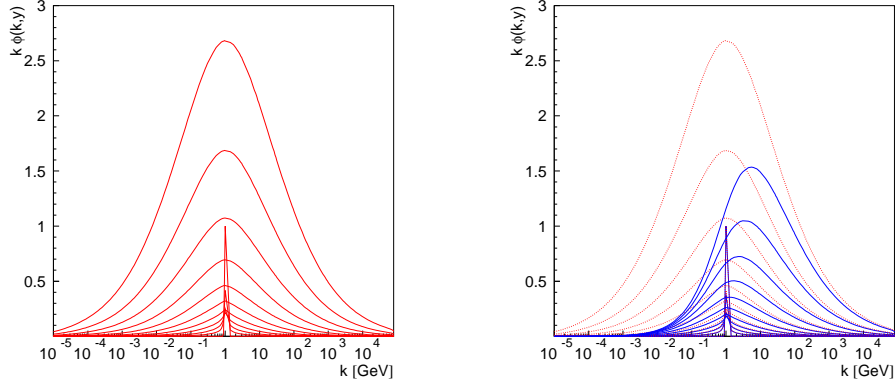


Figure 19: Left: solution to the BFKL equation in the momentum space as a function of momentum k for various fixed values of rapidity $Y = 1, \dots, 10$; right: the same but both BFKL (dashed) and BK (solid) solutions are showed.

momentum space

$$\phi(k, Y) := \int_0^\infty \frac{dr}{r} J_0(k r) N(r, Y) ,$$

in $(1+1)$ dimensions one can obtain a more compact form of this equation

$$\frac{d\phi(k, Y)}{dY} = \bar{\alpha}_s \int \frac{dk'}{k'} \mathcal{K}(k, k') \phi(k', Y) - \bar{\alpha}_s \phi^2(k, Y) . \quad (22)$$

In Eq. (22) the integral operator $\mathcal{K}(k, k')$ is the usual BFKL kernel in momentum space.

The solution to the linear part is well known. In the saddle point approximation it reads

$$k\phi(k, Y) = \frac{1}{\sqrt{\pi\bar{\alpha}_s\chi''(0)Y}} \exp(\bar{\alpha}_s\chi(0)Y) \exp\left(-\frac{\ln^2(k^2/k_0^2)}{2\bar{\alpha}_s\chi''(0)Y}\right) . \quad (23)$$

The first exponential is responsible for the fast increase of the gluon density with rapidity. The value of $\chi(0) = 4 \ln 2$ is the famous BFKL intercept. The second exponential causes the diffusion of the momenta into the ultraviolet and infrared regions. It is well known fact that the BFKL equation exhibits strong diffusion, which can be interpreted as a random walk in the $\ln k$ space of transverse momenta. The rapidity (energy) plays here the role of the time variable. The left plot of Fig. 19 illustrates the numerical solution to the BFKL as a function of transverse momentum for fixed values of Y .

The Gaussian shape predicted by (23) is obvious and the width increases with rapidity. This constitutes a potential problem since while one starts from

a perturbative calculation at a fixed, large scale k_0 , eventually the nonperturbative regime of $\Lambda_{QCD} \sim k \ll k_0$ is reached. This is not the case for the solutions nonlinear BK equation, which are illustrated by solid lines on right plot in Fig. 19. Clearly, in the case of the solutions to the BK equation, the diffusion into the infrared region is strongly suppressed. With increasing Y the distribution peak moves away from the initial value k_0 towards the larger values of k . Therefore one can define saturation scale as a position of the peak

$$Q_s(Y) \equiv k_{\max}(Y) .$$

The suppression of the diffusion can be also visualized with help of the normalized distribution

$$\Psi(k, Y) = \frac{k\phi(k, Y)}{k_{\max}(Y)\phi(k_{\max}(Y), Y)} . \quad (24)$$

On left hand side of Fig. 20 shows the contour plot in (k, Y) space of the distribution (24) for the case of the linear BFKL equation. The contour lines correspond to the constant values of the normalized distribution $\Psi(k, Y)$. The diffusive character of the solution is clearly visible. On the right hand side of Fig. 20 we show the corresponding contour plot for the nonlinear BK equation. We see that the contour lines are shifted towards the higher values of transverse momenta¹. We can also identify a line in (k, Y) space which divides the region where there still is a diffusion (to the right) and where there is no diffusion. The contour lines are parallel to each other in the latter case what means that the solution is scaling there. When the parametrisation $\xi = \ln k/k_0 - \lambda Y + \xi_0$ is introduced the solution depends only on ξ alone. The critical line defines the saturation scale that was introduced in the previous paragraphs. It turns out that the nonlinear BK equation can be approximately treated as a linear diffusion equation with the absorptive boundary close to the critical line defined by the saturation scale $Q_s(Y)$ [21]. This approximation allows us to evaluate precisely the rapidity dependence of the saturation scale.

Recently, there has been quite substantial development achieved towards the understanding of the solutions to the (1+1) dimensional BK equation. In a series of important papers [19] it was proved that BK equation can be approximated as a diffusion equation with a nonlinear term. This makes it equivalent to the Fisher-Kolmogorov-Petrovsky-Piscounov (FKPP) equation [24]

$$\partial_t u(t, x) = \partial_x^2 u(t, x) + u(t, x)[1 - u(t, x)] , \quad (25)$$

where the change of variables from $(Y, \ln k)$ to (t, x) has been performed with simultaneous identification of $\phi \rightarrow u$. FKPP equation has been already studied in many fields of physics, and its solutions are very well understood. In particular it is well known that the FKPP equation has a travelling wave solution for large times (which are equivalent to large energies) which is just a property of geometrical scaling. For a review see for example [25].

¹A distortion of the contours at the highest values of k is unphysical and is caused by cutoffs in numerical calculation.

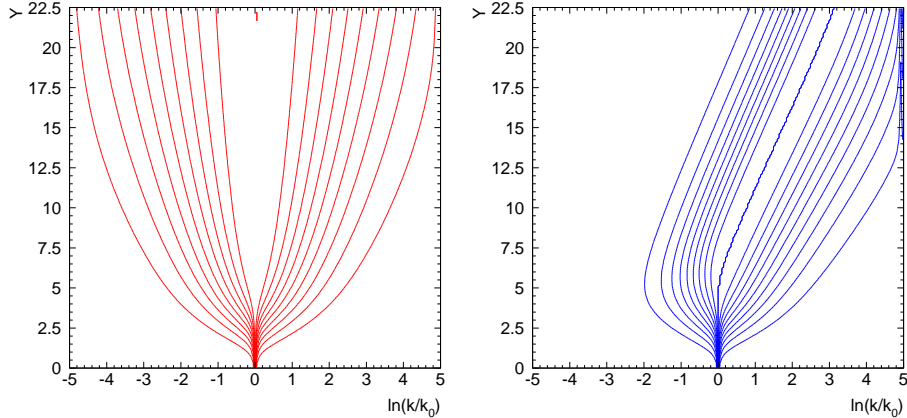


Figure 20: Contour plots of the renormalized distribution $\Psi(k, Y)$ in the case of the linear BFKL solution and the nonlinear BK solution.

9.1 BK equation with running coupling

As we have already stated, the BK equation has been derived within the leading logarithmic in $\ln 1/x$ (LLx) approximation in which the coupling constant is fixed. However, it is very well known fact, that NLLx effects are very important in the BFKL formalism [26]. At NLLx order the coupling runs, and the linear BFKL equation becomes very unstable. The reason is that the linear evolution is very sensitive to the details of the running coupling regularization. This effect is illustrated in Fig. 21 where we show the solution $k\phi^{\text{BFKL}}(k, Y)$ with the running coupling, as a function of the transverse momentum for increasing values of Y . For small values of rapidity the position of the maximum remains close to the value of the initial condition $k = k_0$. However as the rapidity increases the position of the maximum abruptly shifts to the small values of momenta. The actual shape of the solution are critically dependent on the regularized value of the coupling, $k \simeq k_{\text{reg}} \ll k_0$.

With the inclusion of the running coupling the BK equation has the following form

$$\frac{d\phi(k, Y)}{dY} = \bar{\alpha}_s(k) \int \frac{dk'}{k'} \mathcal{K}(k, k') \phi(k', Y) - \bar{\alpha}_s(k) \phi^2(k, Y). \quad (26)$$

The solution to the above equation is illustrated in Fig. 22, superimposed onto the solution of the linear BFKL equation. The solution is much more stable than in the linear case, and the maximum of the distribution is not shifted to the infrared. Instead as rapidity increases, the maximum moves towards the higher values of transverse momenta. The reason for this is that the nonlinear term strongly damps the diffusion into the infrared regime. The saturation scale $Q_s(Y)$ provides a natural cutoff for the low momenta and then no dependence

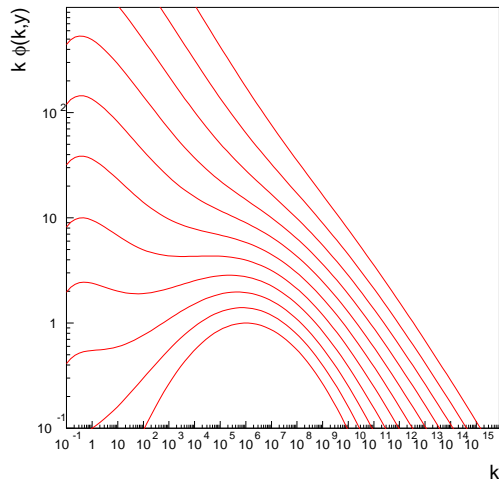


Figure 21: Solution to the BFKL equation with running coupling.

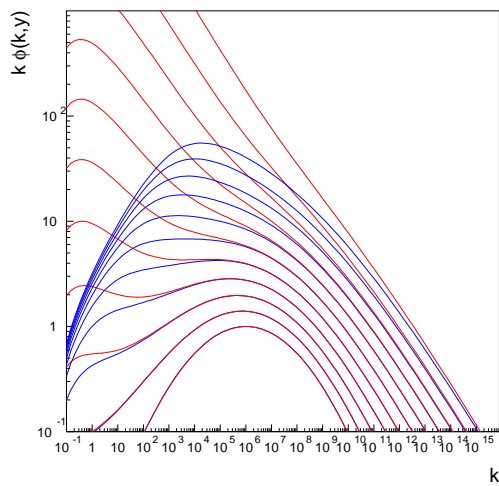


Figure 22: Solution to the BK equation (as compared to BFKL) with running coupling .

on the regularisation of the running coupling is seen (see for example [17, 27, 28, 29]).

One might ask whether the geometrical scaling is still preserved in the presence of the additional scale Λ_{QCD} which is implicitly introduced by use of the running coupling constant. It turns out that the scaling still holds, although the saturation scale has a different rapidity dependence (see [17, 21, 30, 29, 31] and also [2])

$$Q_s(Y) = \Lambda_{QCD} \exp \left(\sqrt{\frac{12c}{\beta_0} (Y - Y_0) + \ln^2 Q_0 / \Lambda_{QCD}} \right), \quad (27)$$

with $c \simeq 2$. The above formula has been derived by assuming that the local exponent of the saturation scale

$$\lambda(Y) = \frac{d \ln(Q_s(Y)/\Lambda)}{dY}$$

has the similar form as in the case of the fixed coupling

$$\lambda(Y) = c \alpha_s(Q_s^2(Y)).$$

By using these two formulae one can derive the saturation scale for the running coupling (27), see [17, 30].

10 Solution in $(3 + 1)$ dimensions

10.1 Spatial distribution: impact parameter dependence

The phenomenon of saturation discussed so far has been based on the properties of the solutions to the BK equation in $1 + 1$ dimensions. Such approach ignores the spatial distribution of the probe-target system. The solution to $(1 + 1)$ dimensional BK equation is integrated over the impact parameter. This is a result of the fact that in $1 + 1$ dimensional case we have assumed an infinite size of the target, and ignored any edge effects. One might expect that the more realistic picture of saturation looks as follows: as the probe collides with the target, a dense system of partons emerges in the limited region of the impact parameter space. For larger impact parameters, the density of partons becomes more and more dilute. The radius of the dense, saturated system expands with the growth of the energy. This process is schematically drawn in Fig. 23. One expects that the impact parameter profile of the scattering amplitude has the behaviour shown in Fig. 24.

A question thus arises whether BK equation can provide information about the impact parameter profile of the amplitude, and whether this profile is consistent with the qualitative picture of saturation. Let us recall the BK equation with full dependence on all coordinates

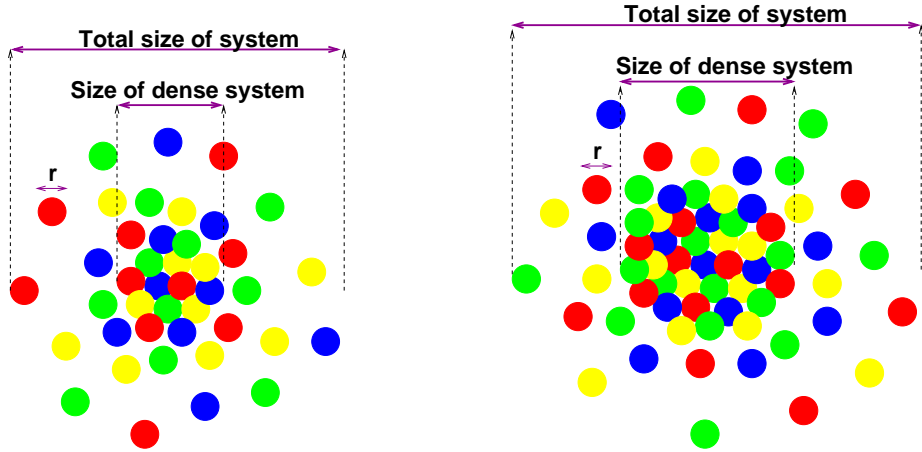


Figure 23: Schematic picture of the impact parameter dependence of the parton density at high energies. Right plot: as energy increases the area of the saturated region, the *black disc*, increases.

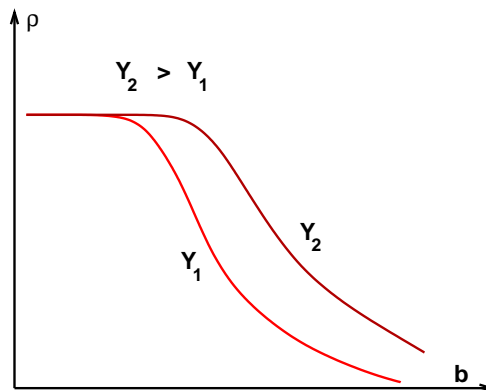


Figure 24: Impact parameter dependence of the scattering amplitude for two different values of rapidity. As energy (rapidity) increases the radius of the saturated plateau also grows.

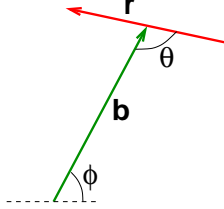


Figure 25: Parametrisation of dipole position.

$$\frac{dN(\mathbf{b}_{01}, \mathbf{x}_{01}, Y)}{dY} = \bar{\alpha}_s \int \frac{d^2 \mathbf{x}_2 \mathbf{x}_{01}^2}{\mathbf{x}_{20}^2 \mathbf{x}_{12}^2} \left[N(\mathbf{b}_{01} + \frac{\mathbf{x}_{12}}{2}, \mathbf{x}_{20}, Y) + N(\mathbf{b}_{01} - \frac{\mathbf{x}_{20}}{2}, \mathbf{x}_{12}, Y) \right. \\ \left. - N(\mathbf{b}_{01}, \mathbf{x}_{01}, Y) - N(\mathbf{b}_{01} + \frac{\mathbf{x}_{12}}{2}, \mathbf{x}_{20}, Y) N(\mathbf{b}_{01} - \frac{\mathbf{x}_{20}}{2}, \mathbf{x}_{12}, Y) \right]. \quad (28)$$

As stated before, in general the problem is very difficult, even numerically, since one has four degrees of freedom per dipole plus rapidity as the evolution variable. Even though the integral measure does not depend on the positions of the dipoles, the impact parameter dependence still exists. It is implicitly generated via the couplings of b_{ij} to x_{ij} in the arguments of the functions N , see Eq. 28. To simplify the problem, and yet retain the information about the impact parameter dependence, we note that measure in the equation

$$\frac{d^2 \mathbf{x}_2 \mathbf{x}_{01}^2}{\mathbf{x}_{20}^2 \mathbf{x}_{12}^2},$$

is invariant under global rotations in transverse space

$$\mathbf{x}_0, \mathbf{x}_1, \mathbf{x}_2 \longrightarrow \mathcal{O}(\phi) \mathbf{x}_0, \mathcal{O}(\phi) \mathbf{x}_1, \mathcal{O}(\phi) \mathbf{x}_2,$$

see Fig. 25.

Therefore one can assume that the position of the dipole is specified by three variables : the dipole size r , the impact parameter b , and the relative orientation of the dipole with respect to the impact parameter axis (angle θ), see Fig. 25. The invariance with respect to global rotations is equivalent to a condition that the target is cylindrically symmetrical. Thus the problem reduces to $(3+1)$ dimensions: $N(r, b, \theta; Y) \rightarrow N(r, b, \theta; Y)$. The BK equation with the impact parameter dependence has been investigated numerically [32, 33], see also [34]. Here we show some of the results taken from [32], which used the initial distribution in Glauber - Mueller form

$$N^{(0)}(r, b, \theta; Y = 0) = 1 - \exp(-r^2 S(b)), \quad (29)$$

where the impact parameter profile has been chosen to be of the Gaussian type

$$S(b) = \frac{1}{R_0^2} \exp(-b^2/b_0^2). \quad (30)$$

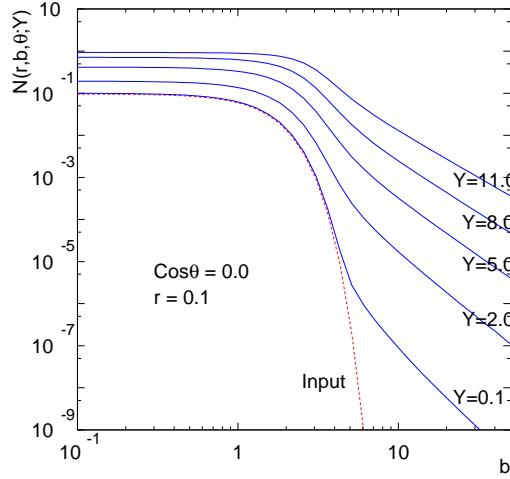


Figure 26: Impact parameter dependence of the solution to the BK equation for increasing values of rapidity.

10.2 Impact parameter dependence

In Fig. 26 we show the resulting impact parameter dependence of the BK solutions calculated for different values of rapidity Y . For small values of b the amplitude is large and strong nonlinear effects are evident. On the other hand, for large values of b one observes a fast growth of the amplitude is governed by the linear part of the equation. One can verify that the increase is exponential in rapidity as expected from the BFKL equation. The region in impact parameter space, where the amplitude is large, expands with growing rapidity. However, perhaps the most striking feature is the fact that the initial profile in impact parameter is not preserved even after a small step in rapidity, $\Delta Y = 0.1$. The exponential tail of the initial distribution immediately assumes power behaviour $\sim 1/b^4$. It is interesting to investigate the origin of these power tails. One can divide the region of integration into long- and short-range parts by introducing a separating cutoff r_0 on the dipole size.

$$\left[\overbrace{\int \Theta(r_0 - |\mathbf{x}_2 - \mathbf{b}|) + \int \Theta(|\mathbf{x}_2 - \mathbf{b}| - r_0)}^{short} \right] \frac{d^2 \mathbf{x}_2 (\mathbf{x}_0 - \mathbf{x}_1)^2}{(\mathbf{x}_0 - \mathbf{x}_2)^2 (\mathbf{x}_1 - \mathbf{x}_2)^2} \cdot \left(N_{02}^{(0)} + N_{12}^{(0)} - N_{01}^{(0)} - N_{02}^{(0)} N_{12}^{(0)} \right).$$

In Fig. 27 the profile in impact parameter space has been decomposed into short and long range contributions. One can see that the short range contribution

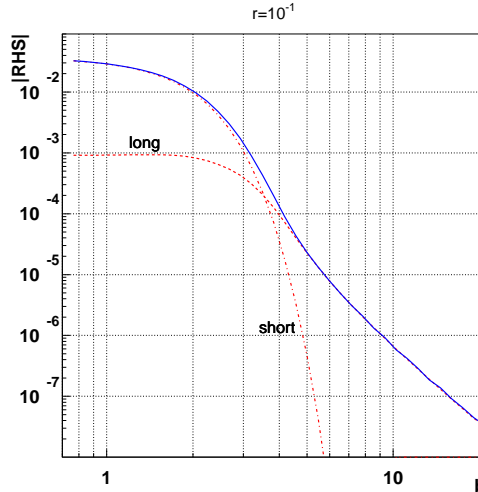


Figure 27: The impact parameter dependence of the amplitude decomposed into the short and long range contributions after small evolution step in rapidity $\Delta Y = 0.1$.

dominates the behaviour at small values of b . There the exponential behaviour is preserved since we have the factorisation of the initial profile $S(b)$ at small values of b . The long range contribution is dominating at large values of impact parameter b where it generates the power tail. Thus the $\sim 1/b^4$ behaviour originates from the integration of the large dipole sizes and is a reflection of the asymptotic behaviour of the integral kernel (see discussion in [35]).

10.3 Violation of Froissart bound

The presence of the power tail in impact parameter has profound consequences for the unitarity. Power decrease of the amplitude means that the interaction is long range. As already stated it, is a direct consequence of the power-like form of the integral kernel

$$\frac{d^2 \mathbf{x}_2 \mathbf{x}_{01}^2}{\mathbf{x}_{20}^2 \mathbf{x}_{12}^2} \simeq d^2 \mathbf{x}_2 \frac{r^2}{b^4}.$$

This type of fast expansion of the interaction system leads to the violation of the Froissart bound, as has been first observed in [35] (compare also a parallel discussion in [36]). It turns out that even though the amplitude is equal or less than 1, due to the nonlinearity of the equation, the dipole cross section increases fast with the decreasing x which violates Froissart bound

$$\sigma = \int d^2 \mathbf{b} N(\mathbf{r}, \mathbf{b}; Y = \ln 1/x) \sim x^{-\lambda}.$$

This happens because the kernel in the BK equation is conformally invariant, with no mass scale which would cut off the long range contributions.

10.4 Dipole size dependence

The dipole size dependence in the case of the impact parameter dependent BK equation is shown in Fig. 28 where the value for the impact parameter has been chosen to correspond to a central collision. For small and moderate values of r it has qualitatively the same behaviour as previously, the amplitude vanishes as r tends to 0 and extends to lower values of r as rapidity grows. It also saturates to 1 for moderate values of r . However, at large values of the dipole size the situation is dramatically different. Here the amplitude drops down again. The reason is that now there is a dimension in impact parameter which characterizes the size of the target. As the dipole grows, at some point it has to completely miss the target and amplitude becomes zero again. This is quite different from the previous case (without the impact parameter) where the amplitude was always saturated since there was an infinite target. It is also interesting to study the solutions at different values of b . In Fig. 29 we present the dipole size dependence of the amplitude for larger value of b which corresponds to a peripheral collision of the dipole with the target. In that case we see that the amplitude peaks for values of the dipole size twice the size of the impact parameter. This is expected, since it reflects the properties of the integral kernel in the BK equation. The solution in the b -dependent case has also several other interesting properties. For values of dipole size much smaller than the impact parameter $r \ll b$, the amplitude depends only on a single combined variable r^2/b^4 . This dependence on one variable, the *anharmonic ratio*, is the result of the conformal symmetry, see for example [11].

10.5 Saturation scale with b dependence

One can also extract the saturation scale from the solution to BK equation in (3+1) dimensions. In [32] a following prescription has been used

$$\langle N(r = 1/Q_s, b, \theta; Y) \rangle_\theta = \kappa, \quad \kappa \sim 0.5. \quad (31)$$

From Fig. 28 we see that the above equation possesses two solutions

$$\frac{1}{Q_s(b, Y)} < r < R_H(b, Y).$$

The lower bound $Q_s(b, Y)$ is the impact parameter dependent saturation scale, which has been plotted in Fig. 30. We see that the saturation scale has strong dependence on b , it is largest at small values of impact parameter and then decreases for large values of impact parameter. The physical picture is that while the impact parameter is increased, one moves from a strongly saturated regime to a more dilute one. The tail of the saturation scale is again power like $\sim 1/b^2$ which is to be expected from the properties of the integral kernel. We

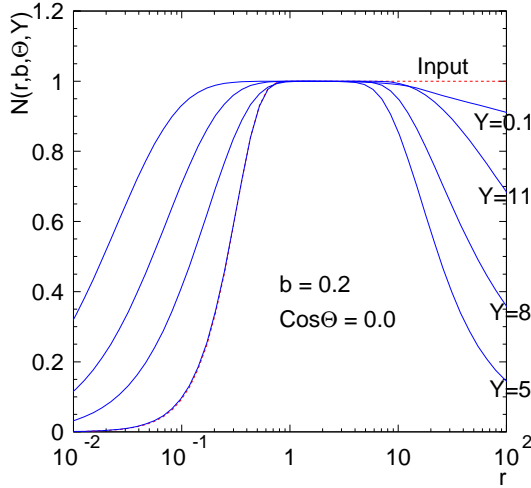


Figure 28: Solution of the impact parameter dependent BK equation with fixed orientation and position of the dipole for various values of rapidity $Y = 0.1, 5, 8, 11$.

see that this behaviour is different from the one that could be anticipated from initial conditions (compare dashed lines). The saturation scale has following behaviour

$$Q_s^2(b, Y) \simeq g(b) \exp(\bar{\alpha}_s 2\lambda_s Y), \quad \lambda_s \simeq 2,$$

where function $g(b)$ is exponentially falling for small values of b and has a power like behaviour at large values of impact parameter.

The second solution $R(b, Y)$ is new compared to the b -independent case, and it just reflects the fact the there is an additional scale present, the finite size of the target.

11 Conclusions and outlook. Beyond BK equation

We have described basic properties of the BK equation which is a nonlinear evolution equation suitable for the description of partonic systems at high density. We have shown that the solution to this equation has a property of geometrical scaling with the characteristic saturation scale. The nice property of this equation is the suppression of the infrared diffusion and independence of the regularization for the running coupling. The impact parameter dependence of this equation leads to the violation of the Froissart bound despite the fact that the amplitude is bounded from above. This is a consequence of purely perturbative approach and the lack of long distance effects such as confinement in the

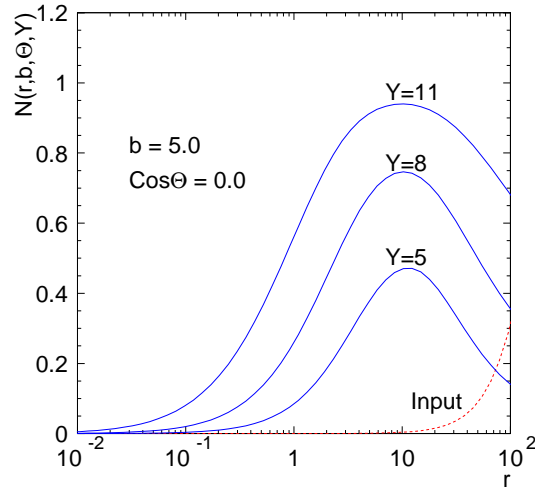


Figure 29: The same as Fig. 28 but for large value of impact parameter $b = 5$.

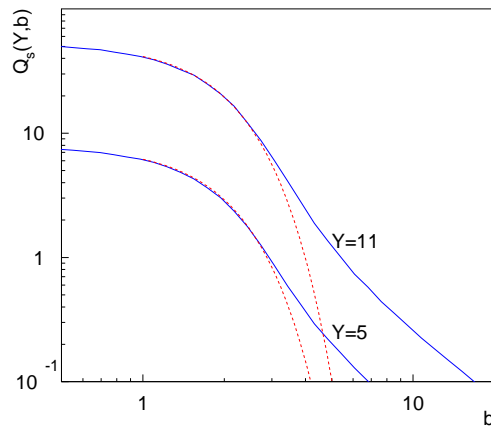


Figure 30: Impact parameter profile of the saturation scale for two various rapidities $Y = 5$ and $Y = 11$. Solid lines are the result of the calculation of full BK equation. Dashed lines correspond to the exponential behaviour of the saturation scale that was expected from initial conditions.

BK equation.

However, the BK equation has been derived by using strong assumptions about lack of correlations in the system and it is thus an equation in mean field approximation. It is not clear to what extent the BK equation is a good approximation to the full Balitsky-JIMWLK equations. In numerical studies of the dipole scattering by Salam [37] it has been shown that the fluctuations are very important and lead to a very different result as compared with the mean field approach. A lot of theoretical effort has been recently devoted to study the role of correlations: in [38] a more quantitative study of the fluctuations has been proposed, in [39] a new equation for the generating functional was postulated which takes into account correlations in the nuclei; in [40] a BK equation with two absorptive boundaries has been studied; in [41] a numerical study of the full JIMWLK equation has been performed for the first time; in [42] an analytical study of the Balitsky hierarchy restricted to the dipole operators, and in [43, 44] the role of the discreteness of the gluon system and connection to the statistical physics have been discussed. We expect that this line of research will be continued in the near future and we will be able to understand the fascinating and complex theory of strong interactions even better.

Acknowledgments

This research is supported by U.S. Department of Energy, Contract No. DE-AC02-98CH10886. I thank Peter Rembiesa for critically reading the manuscript.

References

- [1] L. N. Lipatov, *Sov. J. Nucl. Phys.* **23** (1976) 338;
E. A. Kuraev, L. N. Lipatov and V. S. Fadin, *Sov. Phys. JETP* **45** (1977) 199;
I. I. Balitsky and L. N. Lipatov, *Sov. J. Nucl. Phys.* **28** (1978) 338.
- [2] L. V. Gribov, E. M. Levin and M. G. Ryskin, *Phys. Rep.* **100** (1983) 1.
- [3] M. Froissart, *Phys. Rev.* **123** (1961) 1053; A. Martin, *Phys. Rev.* **129** (1963) 1432. A. Martin, *Phys. Rev.* **129** (1963) 1432.
- [4] L. McLerran and R. Venugopalan, *Phys. Rev.* **D49** (1994) 2233; *ibid.* **D49** (1994) 3352; *ibid* **D50** (1994) 2225;
J. Jalilian-Marian, A. Kovner, L. McLerran and H. Weigert, *Phys. Rev.* **D55** (1997) 5414; R. Venugopalan, *Acta Phys. Polon.* **B30** (1999) 3731;
E. Iancu, A. Leonidov and L. McLerran, *Nucl. Phys.* **A692** (2001) 583;
E. Ferreiro, E. Iancu, A. Leonidov and L. McLerran, *Nucl. Phys.* **A 701** (2002) 489;
E. Iancu and R. Venugopalan, hep-ph/0303204.

- [5] J. Jalilian-Marian, A. Kovner, A. Leonidov and H. Weigert, *Nucl. Phys. B* **504** (1997) 415; *Phys. Rev. D* **59** (1999) 014014. J. Jalilian-Marian, A. Kovner and H. Weigert, *Phys. Rev. D* **59** (1999) 014015.
- [6] H. Weigert, *Nucl. Phys. A* **703** (2002) 823.
- [7] I. I. Balitsky, *Nucl. Phys. B* **463** (1996) 99; I. I. Balitsky, *Phys. Rev. Lett.* **81** (1998) 2024; *Phys. Rev. D* **60** (1999) 014020.
- [8] Yu. V. Kovchegov, *Phys. Rev. D* **60** (1999) 034008.
- [9] A. H. Mueller, *Nucl. Phys. B* **415** (1994) 373
- [10] V.N. Gribov and L.N. Lipatov, *Sov. J. Nucl. Phys.* **15** (1972) 438; Yu.L. Dokshitzer, *Sov. Phys. JETP* **46** (1977) 641; G. Altarelli and G. Parisi, *Nucl. Phys. B* **126** (1977) 298.
- [11] L. N. Lipatov, *Sov. Phys. JETP* **63** (1986) 904.
- [12] S. Munier, A.M. Stasto and A.H. Mueller, *Nucl. Phys. B* **603** (2001) 427.
- [13] K. Golec-Biernat and M. Wüsthoff, *Phys. Rev. D* **59** (1999) 014017; *Phys. Rev. D* **60** (1999) 114023; *Eur. Phys. J. C* **20** (2001) 313.
- [14] M. A. Braun, *Eur. Phys. J. C* **16** (2000) 337.
- [15] N. Armesto, M.A. Braun, *Eur. Phys. J. C* **20** (2001) 517; J.L. Albacete, N. Armesto, A. Kovner, C.A. Salgado, U.A. Wiedemann, *Phys. Rev. Lett.* **92** (2004) 082001; J.L. Albacete, N. Armesto, J.G. Milhano, C.A. Salgado, U.A. Wiedemann, [hep-ph/0408216](http://arxiv.org/abs/hep-ph/0408216).
- [16] M. Lublinsky, E. Gotsman, E. Levin, U. Maor, *Nucl. Phys. A* **696** (2001) 851; M. Lublinsky, *Eur. Phys. J. C* **21** (2001) 513.
- [17] K. Golec-Biernat, L. Motyka, A.M. Stašto, *Phys. Rev. D* **65** (2002) 074037.
- [18] E. Levin and K. Tuchin, *Nucl. Phys. B* **573** (2000) 833; *Nucl. Phys. A* **691** (2001) 779; *Nucl. Phys. A* **693** (2001) 787.
- [19] S. Munier and R. Peschanski *Phys. Rev. Lett.* **91** (2003) 232001; *Phys. Rev. D* **69** (2004) 034008; [hep-ph/0401215](http://arxiv.org/abs/hep-ph/0401215).
- [20] J. Bartels, V. Fadin, L.N. Lipatov, *Nucl. Phys. B* **696** (2004) 255.
- [21] A.H. Mueller and D.N. Triantafyllopoulos, *Nucl. Phys. B* **640** (2002) 331.
- [22] A. Stašto, K. Golec-Biernat and J. Kwieciński, *Phys. Rev. Lett.* **86** (2001) 596.

- [23] N. Armesto, C.A. Salgado, U.A. Wiedemann, [hep-ph/0407018](#); A. Freund, K. Rummukainen, H. Weigert, A. Schafer, *Phys. Rev. Lett.* **90** (2003) 222002.
- [24] R.A. Fisher, *Ann. Eugenics* **7** (1937) 355; A. Kolmogorov, I. Petrovsky and N. Piscounov, *Moscow Univ. Bull. Math.* **A1** (1937) 1.
- [25] W. van Saarloos, *Phys. Rep.* **386** (2003) 29.
- [26] V. S. Fadin, M. I. Kotsky and R. Fiore, *Phys. Lett.* **B 359**, 181 (1995); V. S. Fadin, M. I. Kotsky and L. N. Lipatov, BUDKERINP-96-92, [hep-ph/9704267](#); V. S. Fadin, R. Fiore, A. Flachi and M. I. Kotsky, *Phys. Lett.* **B 422**, 287 (1998); V. S. Fadin and L. N. Lipatov, *Phys. Lett.* **B 429**, 127 (1998); G. Camici and M. Ciafaloni, *Phys. Lett.* **B 386**, 341 (1996); *Phys. Lett.* **B 412**, 396 (1997) [Erratum-*ibid.* B **417**, 390 (1997)]; *Phys. Lett.* **B 430**, 349 (1998).
- [27] M.A. Braun, *Phys.Lett.* B576:115-121,2003.
- [28] J.L. Albacete, N. Armesto, J.G. Milhano, C.A. Salgado, U.A. Wiedemann, [hep-ph/0408216](#).
- [29] D.D. Dietrich, [hep-ph/0411192](#).
- [30] E. Iancu, K. Itakura, L. McLerran, *Nucl. Phys.* **A 708** (2002) 327.
- [31] D.N. Triantafyllopoulos, *Nucl.Phys.* B648 (2003) 293-316.
- [32] K. Golec-Biernat and A.M. Staśto, *Nucl. Phys.* **B 668** (2003) 345.
- [33] E. Gotsman, M. Kozlov, E. Levin, U. Maor, E. Naftali, *Nucl. Phys.* **A 742** (2004) 55.
- [34] T. Ikeda, L. McLerran, [hep-ph/0410345](#).
- [35] A. Kovner and U.A. Wiedemann, *Phys. Rev.* **D 66** (2002) 051502; *Phys. Rev.* **D 66** (2002) 034031; *Phys. Lett.* **B 551** (2003) 311.
- [36] E. Ferreiro, E. Iancu, K. Itakura, L. McLerran, *Nucl. Phys.* **A 710** (2002) 373.
- [37] G.P. Salam, *Nucl. Phys.* **B 449** (1995) 589; *Nucl. Phys.* **B 461** (1996) 512; A.H. Mueller and G.P. Salam, *Nucl. Phys.* **B 475** (1996) 293.
- [38] E. Iancu and A.H. Mueller, *Nucl. Phys.* **A 730** (2004) 494.
- [39] E. Levin and M. Lublinsky, *Nucl. Phys.* **B 370** (2004) 191; [hep-ph/0411121](#).
- [40] A.H. Mueller and A. Shoshi, *Nucl. Phys.* **B 692** (2004) 175.

- [41] K. Rummukainen, H. Weigert, *Nucl. Phys. B* **739** (2004) 183.
- [42] R.A. Janik and R. Peschanski, [hep-ph/0407007](#);
R.A. Janik, [hep-ph/0409256](#).
- [43] E. Iancu, A.H. Mueller, S. Munier, [hep-ph/0410018](#).
- [44] E. Iancu and D.N. Triantafyllopoulos, [hep-ph/0411405](#).